THEORETICA CHIMICA ACTA
Theoret. Chim. Acta (Berl.) 64, 501–514 (1984)

The electronic structure of α-B_{12}, $B_{12}P_2$ and $B_{12}As_2$

David R. Armstrong, John Bolland, and Peter G. Perkins

Department of Pure and Applied Chemistry, University of Strathclyde, Glasgow G1 1XL, Scotland

The electronic band structures of the rhombohedral-based boron compounds α-B_{12}, $B_{12}P_2$ and $B_{12}As_2$ have been investigated along all symmetry directions. The calculations show that the band gap, in all cases, is of the order of 2 eV, which correlates with the known color of α-rhombohedral boron. The materials should be intrinsic semi-conductors, as has recently been shown experimentally. The states around the band gap in α-B_{12} are dominated by the boron $2p$ atomic states. The bonding in the icosahedra, as illuminated by cluster calculations, is shown to be rather similar to that in the isolated B_{12} icosahedron. Of the intericosahedron interactions, those between B(2) and B(2) atoms are the strongest and have a bond index just above unity. In $B_{12}P_2$ the orbitals of the P_2 moiety make a significant contribution to the valence band edge states and the conduction band edge states also incorporate considerable (55%) phosphorus $3d$ orbital character. In $B_{12}As_2$ the arsenic $4d$ orbitals do not have as much effect in that crystal as do the $3d$ orbitals in $B_{12}P_2$.

Key words: Rhombohedral boron compounds—Band structure—Density of states—Cluster model.

1. Introduction

In all allotropes of elemental boron and in a great number of boron-rich compounds, the basic structural unit of the lattice is found to be the B_{12} icosahedral cluster. It is the interconnection of these B_{12} units within the lattice which affords the complex structures of many of these compounds. This complexity arises from the presence of the six five-fold axes of an isolated icosahedron and the alignment of the directed intericosahedral bonds along the axes. A lattice of regular icosahedra cannot be developed over long ranges and hence, for space-filling purposes, the lattice as a whole must relax to a more complex structure.

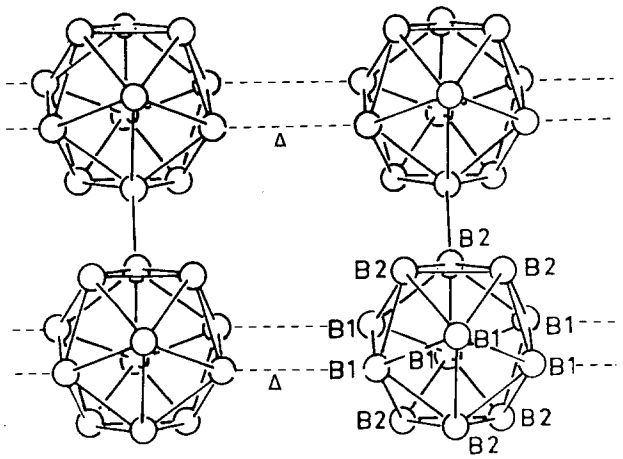

Fig. 1. The structure of B_{12}

The crystal of α-rhombohedral boron consists of B_{12} icosahedra located at the vertices of the rhombohedral cell in such a way that their three-fold axis coincides with that of the rhombohedron and three of the six five-fold axes lie along the edges of the cell. This allows six of the twelve borons to form correctly oriented covalent bonds with atoms on neighboring polyhedra. The boron atoms not involved in interlayer bonding and belonging to adjacent B_{12} units participate in three-centre Δ bonding (see Fig. 1).

In this paper we label the former atoms type 2 (B(2)) and the latter atoms as type 1 (B(1)). This arrangement gives rise to planes of weakly interacting icosahedra vertically connected by B(2)—B(2) bonds and explains the reported anisotropy of α-rhombohedral boron. The presence of Δ bonds accounts also for the low thermal stability and high chemical reactivity of α-B_{12} [1].

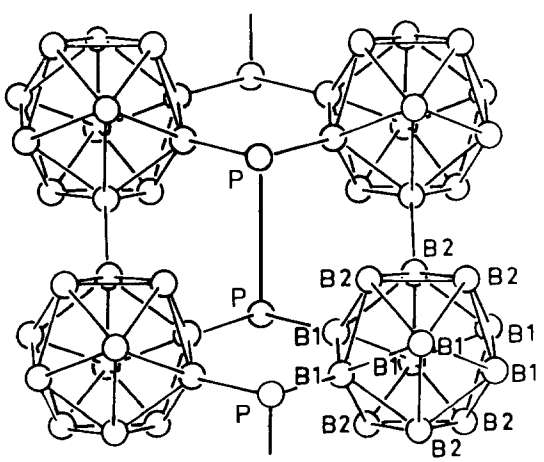

Fig. 2. The structure of $B_{12}P_2$

Other members of this structural family of compounds exist e.g. $B_{12}P_2$ and $B_{12}As_2$. Here the three-centre bonds are replaced by normal covalent bonds to suitably placed heteroatoms which occur in chains within the interstices of the lattice as shown in Fig. 2. These latter compounds are characterised by a framework of rigid covalent bonds and are hard and chemically exceptionally stable. The electronic structure of the related rhombohedral boron carbide, $B_{12}CBC$, has been previously described [2] and the bonding in the crystal and its stoichiometry and properties rationalised. In the present paper we examine the electronic structure of α-B_{12} and two members of the α-rhombohedral boron structural family, $B_{12}P_2$ and $B_{12}As_2$. In particular we concentrate on the bonding pattern of the parent B_{12} compound and the effect of the interstitial chains P_2 and As_2 on the electron distribution and bonding.

2. Calculational method

The solid-state calculational methods used to evaluate the band structure and the density of states of the three species have been described previously [3, 4]. Standard atomic input parameters plus the known crystal structural data were used [5–7]. All three compounds belong to the $R\bar{3}M$ space group and the corresponding rhombohedral Brillouin zone is shown in Fig. 3. In each case, the energy band structure was obtained along the lines *XKΓTWL* and *UXΓLUT*. The bonding in the compounds was also recalculated *via* cluster-model calculations [8] which allows the evaluation of inter- and intra-icosahedral bond indices. The latter quantities are useful in discussion of the relative strengths of chemical bonds.

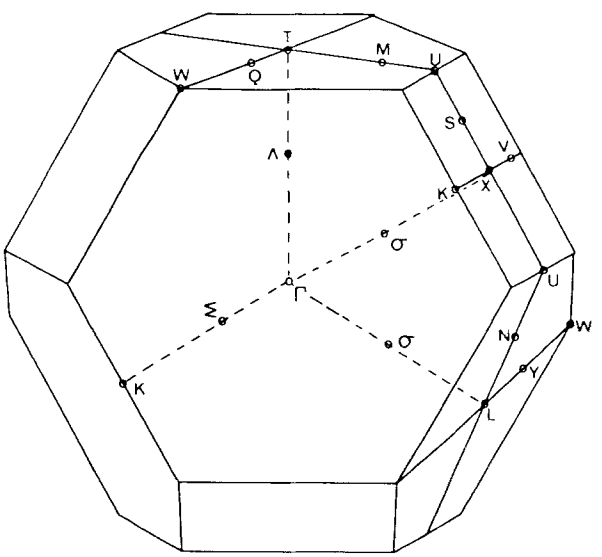

Fig. 3. The Brillouin zone for the rhombohedral Bravais lattice

3. Results and discussion

3.1. α-rhombohedral boron

The band structure of α-B_{12} is shown in Fig. 4. In comparison with the substituted compound $B_{13}C_2$ [2], the band structure exhibits more curvature. This stems from the more delocalised nature of the Δ bonds which involve the B(1) atoms. There are 18 valence bands in α-B_{12} and each band is occupied by two electrons: hence, α-B_{12} is not expected to be an electronic conductor. The valence band edge occurs at the T-point and lies at -5.7 eV, whilst the conduction band edge lies at -3.3 eV along the Δ symmetry line (Γ to T). This affords an indirect band gap of 2.4 eV. A recent investigation [9] of the electrical properties of α-B_{12} has shown that the valence-conduction band gap is 2 eV and this finding is in satisfactory agreement with our results. Both band-edge states are dominated by the B(1)2p orbitals: these are involved in the Δ bonding and are not as strongly

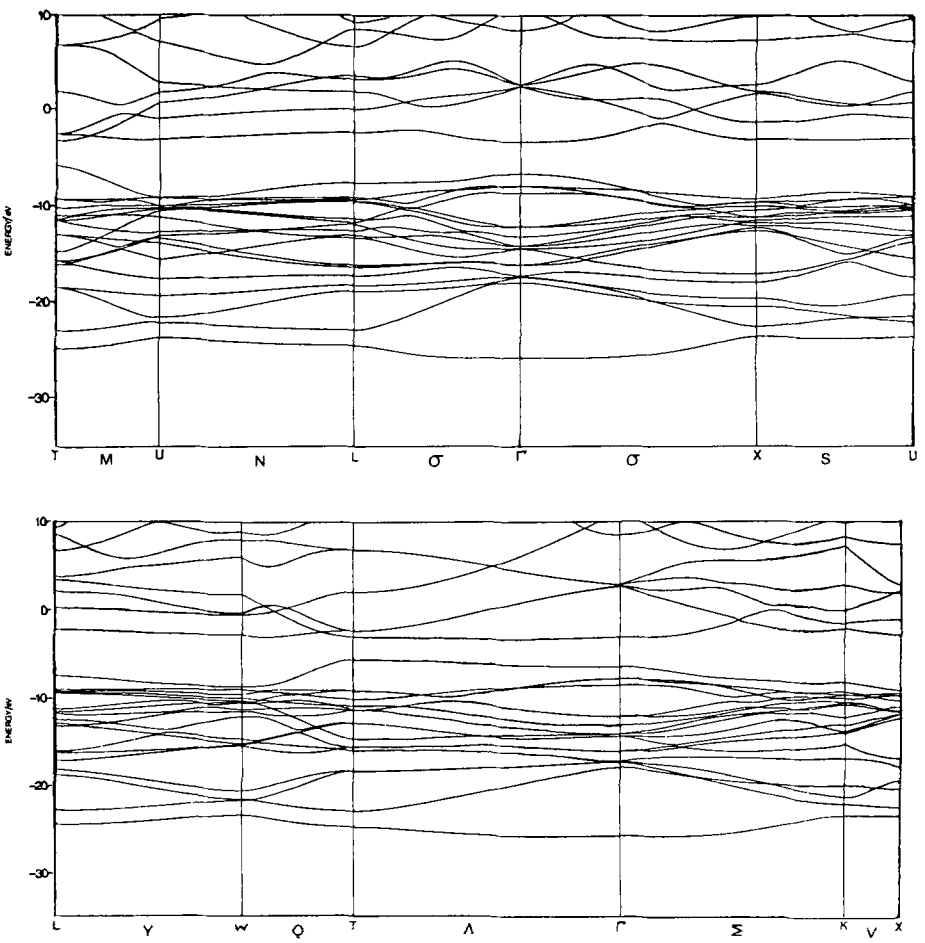

Fig. 4. The band structure for B_{12}

Table 1. Composition of the states at the band edges for B_{12}

	Valence band edge states (%)		Conduction band edge states (%)	
Atom	*s*	*p*	*s*	*p*
B(1)	0.0	79.1	0.8	76.0
B(2)	0.0	20.9	0.1	23.2

split as are other bonding orbitals (see Table 1). Hence, the low-energy transitions in α-B_{12} are not expected to have strong charge-transfer character.

The total density of states and the component partial density of states are shown in Fig. 5. The low-energy end of the energy spectrum (−26.0 to −20.0 eV) is dominated by the boron 2*s* atomic states. This is followed by a region 7 eV wide in which the states consist of boron 2*s* and 2*p* orbitals. Finally, the high-energy section contains pure boron 2*p* states. The occupied boron 2*p* atomic states span a region 15.8 eV wide and stretching from −5.7 eV to −21.5 eV. This result agrees well with the experimental estimate of 15.5 eV stemming from X-ray emission techniques [10]. In the emission spectrum of α-B_{12}, three prominent peaks are manifest. In Fig. 5, the three calculated peaks (a–c, Fig. 5) exhibit mutual energy separations 3 eV and 4.2 eV and this is in fair agreement with the experimental differences of 4 eV (a–b) and 5 eV (b–c), respectively. The joint density of states, which can be roughly correlated with the absorption spectrum, shows that radiation of energy greater than 2.4 eV will be absorbed by α-B_{12}. In the energy region 2.4 to 10.0 eV continuous absorption is predicted, with maxima in the JDOS function occurring at 6.7 eV, 7.3 eV, and 8.1 eV. The lowest absorption limit is consistent with the observed red color of the α-B_{12} crystals.

The electron distribution for α-B_{12} can be obtained from the density-of-states calculation in which the electron population of each state is partitioned with respect to the component orbitals. It is also available from a cluster calculation [8] where a portion of the crystal is treated to a pseudo-molecular calculation. The resulting electron densities, bond indices and valencies of B_{12} are collected in Table 2. Both sets of calculations produce essentially the same charge distribution; there is a small electron flow from the B(1) (equatorial) atoms to the B(2) (polar rhombohedral) atoms. This electron-density difference is related to differing 2*p* populations. The B(2) atoms form stronger bonds than do the B(1) atoms and, hence, are associated with more electron density. The partial density-of-states plots, especially near 8.5 eV, illustrate this point: there are more occupied B(2) states than B(1) states. The 2*s* electron populations of the boron atoms are unusually low and this feature is related to the multibonding nature of the boron atoms.

Each atom in the B_{12} icosahedron forms five icosahedral bonds, each with a bond index of *ca.* 0.5. The strongest of these bonds is the B(1)—B(2) interaction connecting a polar triangular atom B(2) to the equatorial atom B(1), while the polar triangular bonds of B(2)—B(2)-type are the weakest. The intericosahedral

interactions are of two types: firstly, the covalent B(2)—B(2) bonds exhibit slight multiple-bond character (bond index = 1.097) and, clearly, are the strongest bonds present in the unit cell. The second type of intericosahedral bond is the Δ bond, where each of the three B(1)—B(1) bonds has an index of 0.45. From

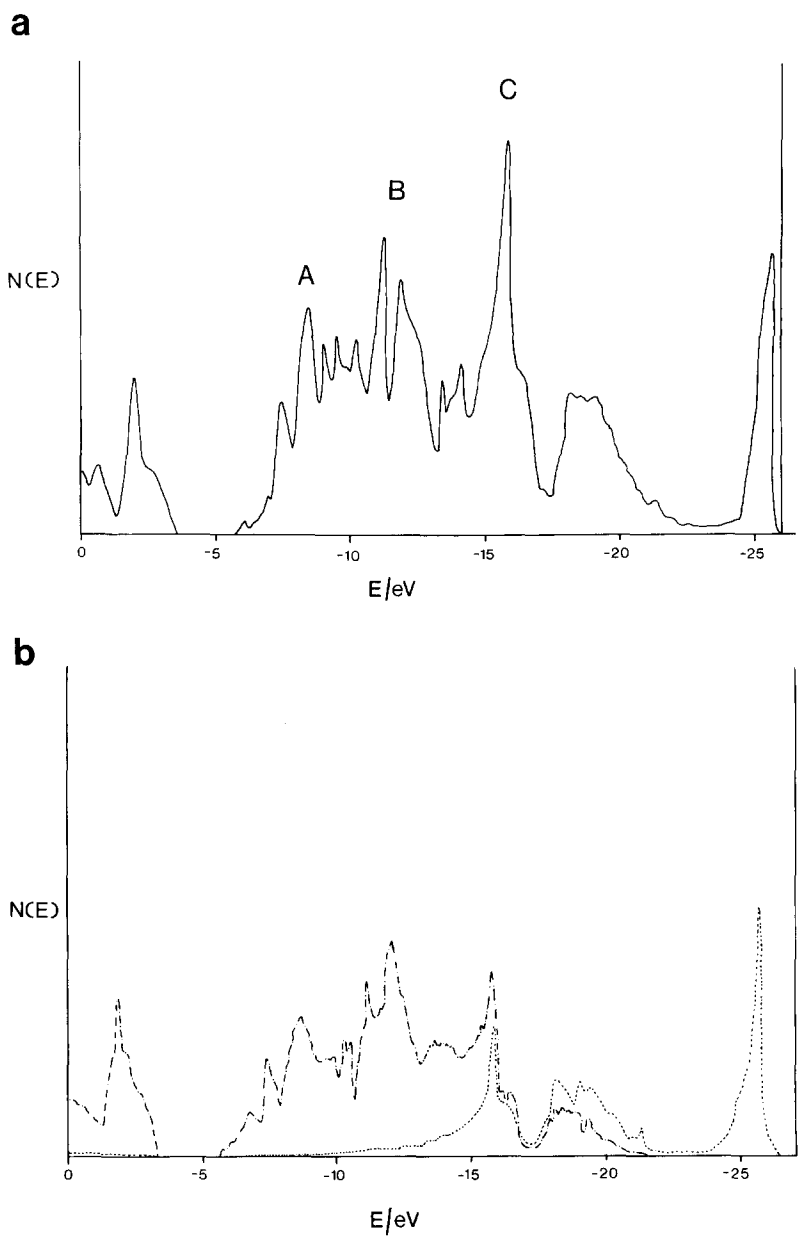

Fig. 5a–c. Density of states for B_{12}, (a) total density of states (b) partial density of states for B(1) atoms and (c) partial density of states for B(2) atoms (· · · · · 2*s* contribution, - - - - - 2*p* contribution)

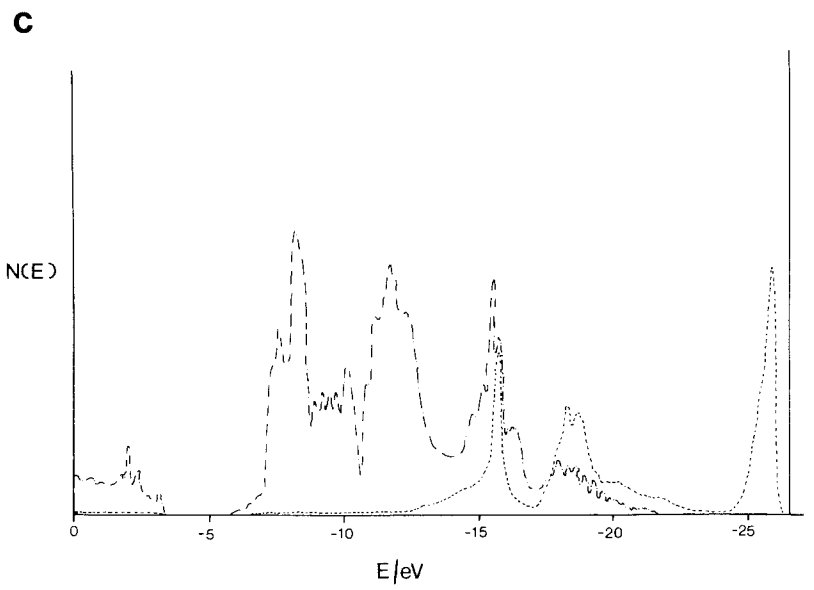

Fig. 5c

Table 2. Electron distribution in α-B_{12}

Electron densities	Atom	*s*	*p*	Total	Charge
Density-of-states	B(1)	0.82	2.02	2.84	0.16
Calculation	B(2)	0.85	2.31	3.16	−0.16
Cluster	B(1)	0.66	2.24	2.90	+0.10
Calculation	B(2)	0.67	2.43	3.10	−0.10
Bond indices[a]					
	B(1)—B(1)	0.52			
	B(1)—B(2)	0.54, 0.51			
	B(2)—B(2)	0.44			
	B(1)—B(1)′	0.45			
	B(2)—B(2)′	1.10			
Valencies					
	B(1)	3.64			
	B(2)	3.71			

[a] Obtained from a cluster calculation

previous work [11] in which the bond strength of boron–boron bonds was related to their bond indices, we can evaluate the energy of a Δ bond as 32.0 kcal and so the bond energy is obviously an important contribution to the overall energy of the B_{12} unit cell.

The valency of an atom is defined to reflect the total bonding of the atom in any situation. It is calculated as the sum of all bond indices emanating from the atom [12, 13]. The valencies of B(1) and B(2) show that the boron atoms fully utilise

the four valence orbitals at their disposal. The polar atoms, B(2), manifest a larger valency than the equatorial boron atoms. This arises from the presence of stronger intericosahedral bonds radiating from the B(2) atoms and these more than compensate for the smaller sum of the B(2) intraicosahedral bonds. Hence, equatorial atoms are expected to furnish reactive positions as their total bonding power is less and their intericosahedral bonds can be more easily ruptured thermodynamically.

3.2. *α-rhombohedral* $B_{12}P_2$.

The band structure of $B_{12}P_2$ is given in Fig. 6. The unit cell has 46 valence electrons and there exists a small band gap between the 23rd and 24th bands throughout the Brillouin Zone. The valence band edge occurs at the Γ-point at −6.7 eV, whilst the lowest conduction band states lie at the symmetry point *L* with an energy of −4.2 eV. Thus, there is an indirect band gap of 2.5 eV. The

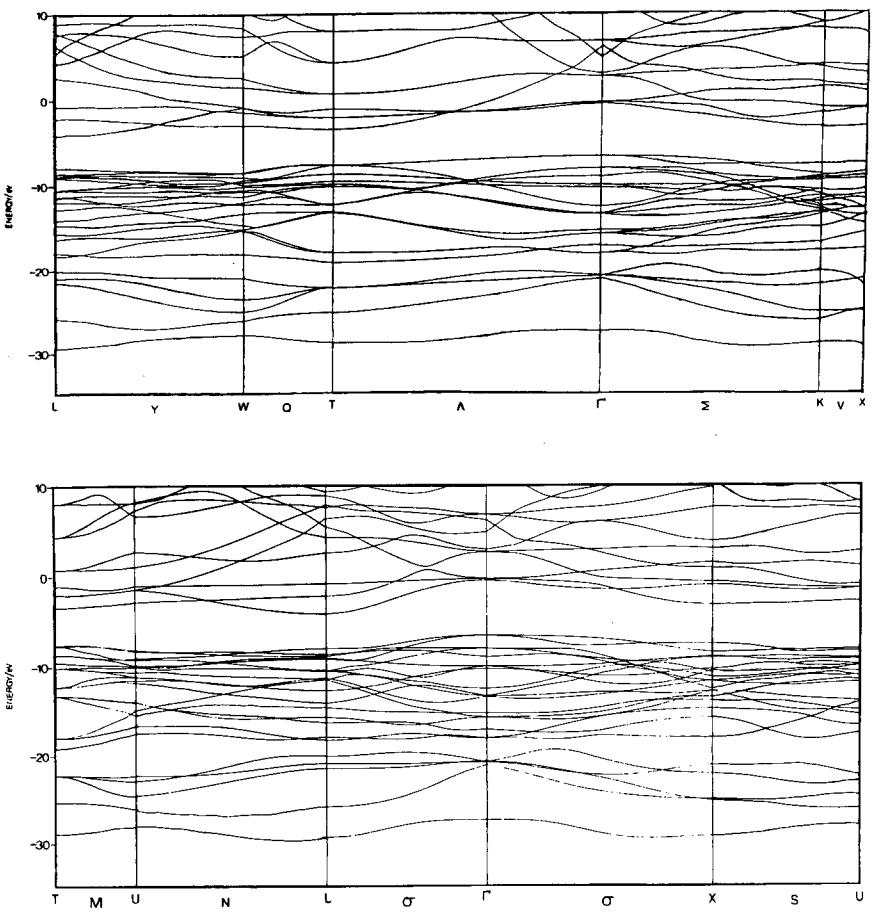

Fig. 6. The band structure for $B_{12}P_2$

Table 3. Percentage composition of the states at the band edges for $B_{12}P_2$

	Valence band edge states (%)			Conduction band edge states (%)		
Atom	*s*	*p*	*d*	*s*	*p*	*d*
B(1)	0.1	57.5	—	0.2	37.3	—
B(2)	0.0	23.0	—	1.1	6.7	—
P	0.0	14.8	4.7	1.1	7.1	46.4

bands in $B_{12}P_2$ possess similar curvature to those in the parent compound B_{12} and contrast with the rather flatter bands in $B_{13}C_2$. Hence, one expects the bonds to be less localised than in the latter system. As the calculated band gap of $B_{12}P_2$ is similar in value to that in B_{12}, the semi-conducting properties and spectral absorption edge of the two systems are predicted to be closely similar. The JDOS plot for $B_{12}P_2$ reveals that the absorption edge lies at 2.5 eV and continuous absorption throughout the remaining visible and ultraviolet region of the spectrum should occur. Maxima in the JDOS plot occur at similar positions to the peaks already extant in the B_{12} JDOS curve.

The composition of the band-edge states is given in Table 3. The major orbital contribution to the valence band-edge states arises from the B(1)2*p* orbitals (as in B_{12}). The orbitals of the P_2 moiety make a significant contribution (~20%) to the valence band-edge states and this causes shifting of the highest filled level from −5.7 eV in B_{12} to −6.7 eV in $B_{12}P_2$. The conduction band-edge states also

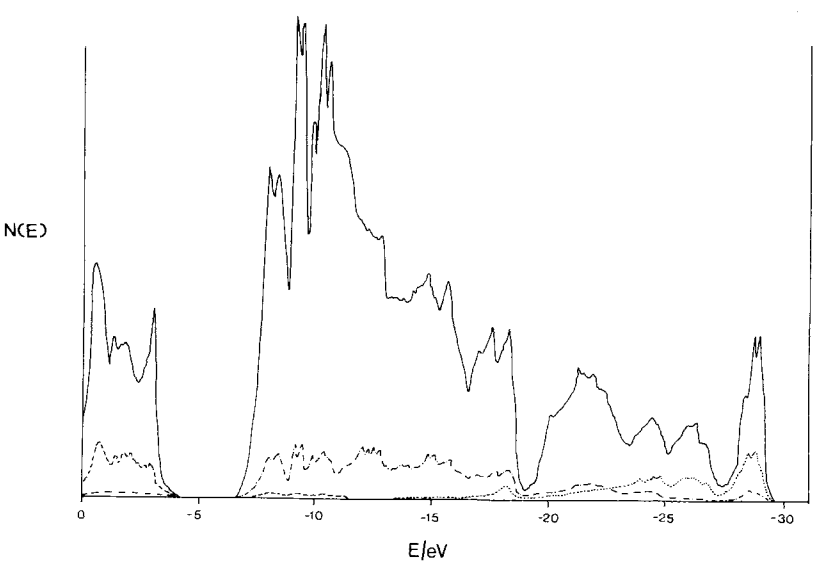

Fig. 7. Density of states for $B_{12}P_2$ (· · · · · P 3*s* contribution, - · - · - P 3*p* contribution, - - - - P 3*d* contribution)

incorporate high (*ca* 55%) phosphorus 3*d* orbital content which lowers the corresponding α-B_{12} level by 0.9 eV.

The total density-of-states plot of $B_{12}P_2$ is given in Fig. 7. The region between −19 eV and −30 eV is populated by boron *s* states, whilst the higher-energy states up to the Fermi edge are predominantly *p* orbital in character. This is illustrated by the %*p* character in the main peaks of the density-of-states plot and relevant data are given in Table 4. The contribution to the density of states of the phosphorus orbitals can be seen from inspection of Fig. 7. There is a high concentration of phosphorus 3*s* states at the low end of the eigenvalue spectrum. The topography of the phosphorus 3*p* states plot is similar to that of the total density-of-states graph indicating that delocalised boron-phosphorus bonding takes place in $B_{12}P_2$.

The phosphorus 3*d* orbitals participate to a limited extent in the higher-energy valence states but are particularly important in the conduction states. The partial-density-of-states curves for B(1) and B(2) (not shown in Fig. 7) resemble closely those of the parent B_{12} crystal, with highly concentrated states lying close to −10 eV. The maximum for the B(2) states lies at lower energy than that of the B(1) states and so, despite the presence of B(1)-P bonds, the states formed from B(2) atoms remain the more stable.

The electron-density distribution for B_{12} resulting from a cluster calculation is given in Table 5. Electrons drift from the P_2 species to the icosahedral unit, resulting in negative charges on all the icosahedral boron atoms: of these the B(2) atoms carry the greater charge. If we compare these atom charges with the corresponding values for B_{12}, it is found that the inclusion of the P_2 unit, and the consequent formation of B(1)—P bonds, raises the charge on the B(1) atoms by 0.13 electrons, whilst the B(2) atoms take on an extra 0.04 electrons. The boron 2*s* orbital occupancies of $B_{12}P_2$ are low, as found for B_{12} itself. It appears, therefore, that the boron 2*p* orbitals also play a critical rôle in the bonding in $B_{12}P_2$.

Each boron atom is bonded to five other boron atoms of the icosahedron with a bond index close to 0.5. In addition, each boron atom is bonded to an atom outwith the icosahedron with a bond index near unity. Hence, the valencies of the boron atoms in $B_{12}P_2$ indicate a near-maximum use of their valence orbitals.

Table 4. *p*-State contributions to the peaks of the density-of-states curve of $B_{12}P_2$

Energy of peak (eV)	Percentage of *p*-states
−8.0	96
−9.3	96
−10.3	96
−14.5	54
−17.5	41
−21.0	11
−28.0	6

Table 5. Cluster calculation electron distribution for $B_{12}P_2$

Atom	*s*	*p*	*d*	Total	Charge
Electron densities					
B(1)	0.51	2.51	—	3.02	−0.02
B(2)	0.70	2.46	—	3.16	−0.16
P	0.96	2.97	0.53	4.46	+0.54
Bond indices					
B(1)—B(1)	0.45				
B(1)—B(2)	0.51, 0.48				
B(2)—B(2)	0.50				
B(2)—B(2)′	0.98				
B(1)—P	1.00				
P—P	1.03				
Valencies					
B(1)	3.62				
B(2)	3.75				
P	4.90				

The phosphorus 3*s*-orbital occupancy is lower than that for atomic phosphorus and this reflects the bonding character of the phosphorus atoms: these are bonded to three B(1) atoms and a P atom in $B_{12}P_2$. It appears that the phosphorus 3*d* orbitals do not play a major rôle in the bonding in $B_{12}P_2$. The principal index of their presence is the P—P bond, for which the bond index is increased from 0.78 to 1.03 by 3*d* orbital inclusion. Other bonds are only marginally affected by the inclusion of the 3*d* orbitals on the phosphorus atoms. The valency of the phosphorus atoms lies close to 5 and results from the participation in four strong bonds plus other, weaker bonds, to the non-neighboring boron atoms.

3.3. α-rhombohedral $B_{12}As_2$

The electronic structure of $B_{12}As_2$ is found to resemble that of $B_{12}P_2$ and for brevity, we summarise our findings here. The band structure of $B_{12}As_2$ is shown in Fig. 8. There are 23 filled bands separated from the conduction bands by a gap of at least 2.3 eV. Thus, $B_{12}As_2$, along with $B_{12}P_2$ and B_{12}, should be a semiconductor. The valence bands are mostly flat, whilst the conduction bands are relatively broad. The highest filled level of $B_{12}As_2$ is found at the Γ-point and has energy −7.3 eV, whilst the lowest vacant level has energy −5.0 eV (at the *L*-point). These two energy levels lie lower than those corresponding for $B_{12}P_2$. The composition of the band-edge states is detailed in Table 6. The valence band-edge states contain large contributions from the B(1)2*p* orbitals, together with a small contribution from the B(2) and As valence *p* orbitals. The conduction band-edge states have two main components; i.e. the B(1)2*p* orbitals and the As 4*d* orbitals. The JDOS plot indicates that absorption will be continuous over the energy range 2.3 to 10 eV, with maxima at 7.1 eV and 7.8 eV.

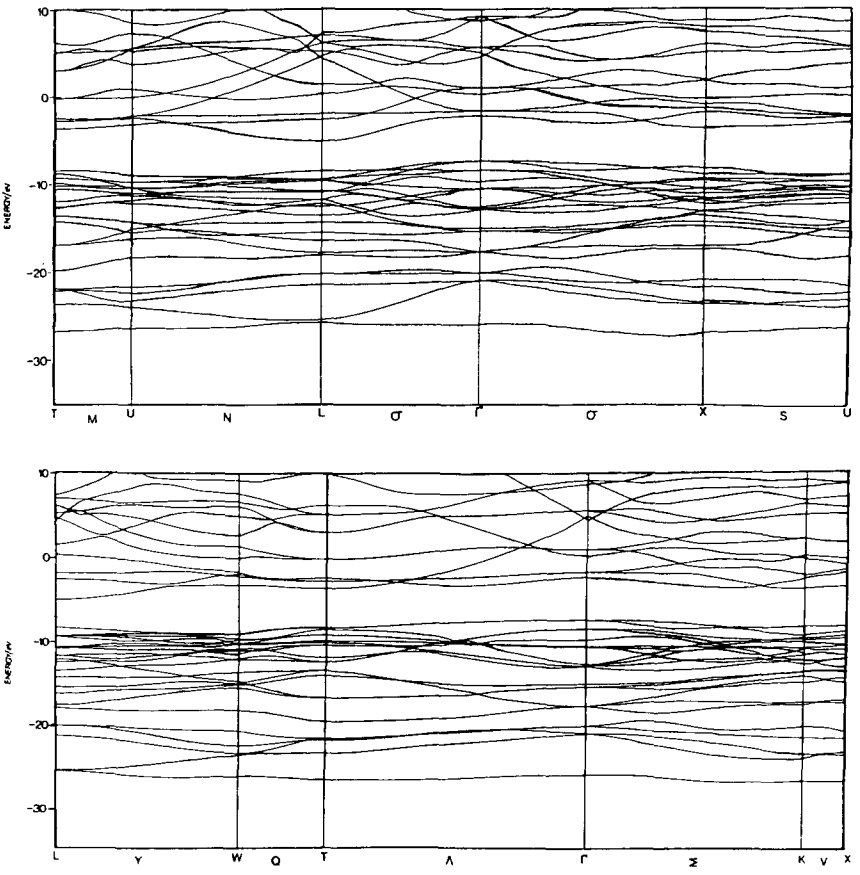

Fig. 8. The band structure for $B_{12}As_2$

Table 6. Composition of the states at the band edges for $B_{12}As_2$

	The valence band edge states (%)			The conduction band edge states (%)		
Atom	*s*	*p*	*d*	*s*	*p*	*d*
B(1)	0.1	53.9	—	0.4	37.9	—
B(2)	0.1	22.2	—	1.0	5.5	—
As	0.0	20.2	3.4	1.1	16.4	37.6

The total density-of-states plot of $B_{12}As_2$ is presented in Fig. 9. The range of the filled bands is narrower than that of $B_{12}P_2$ and this can be attributed to the lower energy of the 4*s* electrons of arsenic.

The position and nature of the peaks in the plot are very similar to those of $B_{12}P_2$, and the distribution of the arsenic valence orbitals throughout the states also parallels that of the phosphorus orbitals in $B_{12}P_2$.

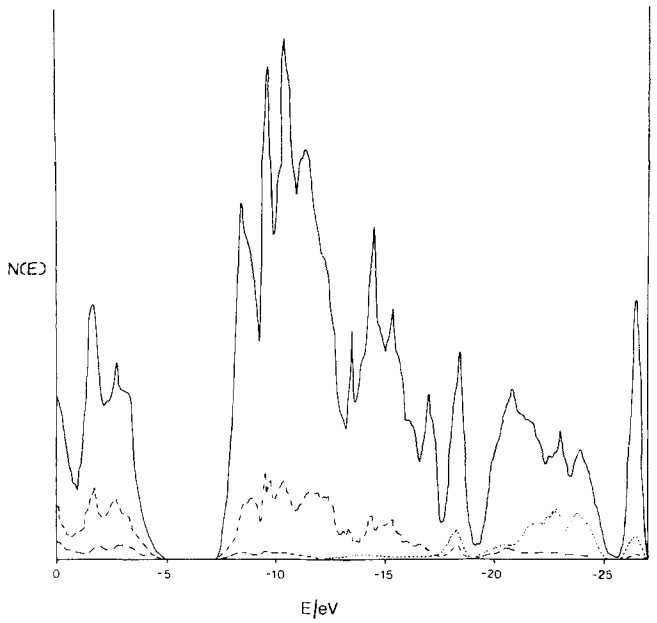

Fig. 9. Density of states for $B_{12}As_2$ (· · · · · As 4*s* contribution, - · - · - As 4*p* contribution, - - - - As 4*d* contribution)

Table 7. Cluster calculation electron distribution for $B_{12}As_2$

Atom	*s*	*p*	*d*	Total	Charge
Electron densities					
B(1)	0.58	2.43	—	3.01	−0.01
B(2)	0.72	2.47	—	3.19	−0.19
As	1.24	2.97	0.21	4.42	+0.58
Bond indices					
B(1)—B(1)	0.50				
B(1)—B(2)	0.53, 0.50				
B(2)—B(2)	0.52				
B(2)—B(2)′	0.98				
B(1)—As	0.98				
As—As	0.83				
Valencies					
B(1)	3.69				
B(2)	3.78				
As	4.32				

The electron distribution for $B_{12}As_2$, obtained from a cluster calculation, is detailed in Table 7. There is, overall, electron donation (1.15 electrons) to the B_{12} icosahedron from the As_2 sub-unit. The B(2) atoms carry a much greater negative charge, even though the B(1) atoms gain more charge from the As_2 species.

The bond indices for the intraicosahedral bonds in $B_{12}As_2$ are slightly greater than in $B_{12}P_2$ but the converse is true of the intericosahedral bonds. The valency of arsenic in the crystal is much lower than that for phosphorus in $B_{12}P_2$. This is related to the higher *s* valence population of As and the consequent lower bond indices for bonds emanating from As. The 4*d* orbitals play a less significant rôle in the bonding of $B_{12}As_2$ than do their 3*d*-orbital counterparts in $B_{12}P_2$. Their intrinsic population is less than half that of the corresponding phosphorus 3*d* orbital population and the *d*—*d* contribution to the As—As bond is smaller than that for the P—P bond.

Acknowledgement. One of us (J.B.) thanks the SERC for a Maintenance Grant.

References

1. Naslain, R.: Boron and refractory borides, p. 139. Matkovich, V. I., ed. Berlin: Springer-Verlag 1977
2. Armstrong, D. R., Bolland, J., Perkins, P. G., Will, G., Kirfel, A.: Acta Cryst. **B39**, 324 (1983)
3. Armstrong, D. R., Breeze, A., Perkins, P. G.: J. Phys. **C.8**, 3558 (1976)
4. Armstrong, D. R., Breeze, A., Perkins, P. G.: J. Chem. Soc. Faraday Trans II **73**, 952 (1977)
5. Decker, B. F., Kasper, J. S.: Acta Cryst. **B12**, 503 (1959)
6. Amberger, V. E., Rauk, P. A.: Acta Cryst. **B30**, 2549 (1974)
7. Amberger, V. E., Rauk, P. A.: Acta Cryst. **B32**, 972 (1976)
8. Perkins, P. G., Stewart, J. J. P.: J. Chem. Soc. Faraday II **76**, 520 (1980)
9. Golkova, O. A., Solovev, N. E., Ugai, Ya. A., Feigelman, V. A.: J. Less-Common Metals **82**, 362 (1981)
10. Domashevskaya, E. P., Soloviev, N. E., Terekov, V. A., Ugai, Y. A.: J. Less-Common Metals **47**, 189 (1976)
11. Laurie, D., Perkins, P. G.: Inorg. Chim. Acta, in press
12. Armstrong, D. R., Perkins, P. G., Stewart, J. J. P.: J. Chem. Soc. Dalton 838 (1973)
13. Armstrong, D. R., Perkins, P. G., Stewart, J. J. P.: J. Chem. Soc. Dalton 2273 (1973)

Received April 25, 1983